Received: 14 May 2020 | Revised: 7 August 2020 | Accepted: 23 August 2020

DOI: 10.1002/pc.25803

RESEARCH ARTICLE

Polymer COMPOSITES WILEY

Real time uncertainty estimation in filling stage of resin transfer molding process

K. I. Tifkitsis | **A. A. Skordos**

School of Aerospace, Transport and Manufacturing, Cranfield University, Bedford, UK

Correspondence
K. I. Tifkitsis, School of Aerospace, Transport and Manufacturing, Cranfield University, Bedford, MK43 0AL, UK.
Email: k.tifkitsis@cranfield.ac.uk

Funding information
Cranfield University; EU

Abstract

This paper addresses the development of a digital twin, based on an inversion procedure, integrating process monitoring with simulation of composites manufacturing to provide a real time probabilistic estimation of process outcomes. A computationally efficient surrogate model was developed based on Kriging. The surrogate model reduces the computational time allowing inversion in real time. The tool was implemented in the filling stage of an resin transfer molding processing of a carbon fiber reinforced part resulting in the probabilistic prediction of unknown parameters. Flow monitoring data were acquired using dielectric sensors. The inverse scheme based on Markov Chain Monte Carlo uses input parameters, such as permeability and viscosity, as unknown stochastic variables. The scheme enhances the model by reducing model parameter uncertainty yielding an accurate on line estimation of process outcomes and critical events such as racetracking. The inverse scheme provides a prediction of filling duration with an error of about 5% using information obtained within the first 30% of the process.

KEYWORDS

process modeling, process monitoring, resin flow, resin transfer molding (RTM)

1 | INTRODUCTION

The lack of full automation and digital manufacturing combined with the inherent process uncertainty[1] involved in composites manufacture increase process complexity and risk introducing variations of process outcomes and potential defects formation. Conservative processes are selected to prevent risks associated with input parameters uncertainty resulting in increased manufacturing costs. The continuous demand for cost reduction and accomplishment of the desired final part quality with zero defects has motivated the development of predictive simulation tools, process monitoring, and automation of composites manufacture. The main objectives of designing a composite manufacturing process are the minimization of process duration and manufacturing cost and the delivery of the desirable product quality. Part quality is characterized by fulfillment of design tolerances, surface state and absence of process-induced defects.

Resin transfer molding (RTM) is a typical example of composites manufacturing processes, in which resin impregnates a dry preform under flow-driving pressure gradient in a sealed rigid mould followed by curing at elevated temperature. Processing decisions such as inlet and outlet locations and injection pressure are crucial for the quality of the final part. The impregnation stage of

composites manufacture presents considerable variations in boundary conditions and material properties.[1] The variability can lead to significant variations in filling duration and initiate process defects such as dry spots and voids resulting in rejected parts. The permeability of textiles is a crucial material property that affects the filling step in liquid composite molding (LCM). Evaluating the permeability of fabrics and its variability is critical as this parameter controls the occurrence of potential problems during impregnation such as dry spots, non-uniform filling, and resin rich zones.[2] Variations in fiber architecture due to handling and storage, nesting effects during lay-up and preform misplacement in the mould affect significantly the permeability values.[3,4] Permeability can show significant variations at the macro and micro scale.[5,6] In the mesoscale the minimum dimensional domain shaping a repeatable representative cell of the fabric level, permeability variations can be represented by a log-normal distribution in the cases of random mat and automated dry fiber placement (ADFP) preforms, where the coefficient of variation of permeability across repeat tests can reach up to 20%.[7,8] Statistical characterization of a glass fiber woven fabric principal permeabilities indicates a Gaussian distribution with a coefficient of variation of about 20%.[9] Repeat rheology experiments have shown considerable variations in the initial state of resin viscosity of epoxies due to difference in shelf life at ambient temperature.[10] Stochastic simulation of LCM has shown that variability of resin viscosity, preform permeability and length of the distribution medium can introduce up to 20% variance in filling duration.[10,11] Variations in through thickness permeability result in high scatter in dry spot content.[12] The apparent permeability values caused by race tracking effects can be represented by a Weibull[13] or normal distribution.[14] The use of the Wiebull distribution offers greater flexibility with respect to the shape and symmetry properties of the probability density function. The measured variations of race tracking permeability highlight the stochastic nature of edge effects and their influence on filling introducing significant variability in resin flow front patterns.[14] Race tracking depends on resin viscosity and its variability can result in undesirable filling patters and thus potential void formation or dry spots. However, only permeability variations have been quantified experimentally, whilst for viscosity which plays a dominant role in flow processes only assumptions have been made related to its variability.[11,15] This is important for the comprehensive investigation of input parameters variability influence on filling stage outcomes.

Important process parameters and material properties such as permeability and viscosity cannot be evaluated in situ during the filling stage of an RTM process due to the constraints of the process. Activity in this area in the literature has focused only on off-line property identification such as preform permeability, viscosity and thermal properties. Flow process monitoring techniques such as lineal sensors have been developed to access filling stage process information such as flow front position assisting in address of undesirable filling behavior such as racetracking effects, formation of dry spots and incomplete filling.[16,17] The on-line integration of process simulation models with process sensing systems requires successful implementation of an inverse solution scheme. Estimation algorithms based on gradient methods of minimization have been implemented combining numerical models with process monitoring data for the online characterization of permeability[18–20] and the estimation of flow front position[21,22] and of resin thermal properties.[23] However, gradient methods of minimization cannot deal fully with the potentially ill posedness of inverse problems of this type. Inverse algorithms such as the Markov Chain Monte Carlo (MCMC) method can address ill-posed problems through the regularization of the solution implied using a prior estimate. MCMC operates as a sampler computing the uncertainty associated with the estimation by incorporating process monitoring measurements and modeling into the inverse scheme.

In the present study, an inverse scheme is developed incorporating flow monitoring with filling simulation for the probabilistic estimation of stochastic parameters and in turn of filling duration and flow front position. Lineal dielectric sensors are placed in strategic positions in the mould cavity providing data during the flow stage. Surrogate filling models based on Kriging are utilized to represent the response of sensors allowing the real time implementation of the inverse scheme. The inverse scheme is implemented and validated for the case of RTM filling of a composite flat panel with a recessed edge.

2 | METHODOLOGY

2.1 | Processing

RTM was utilized for the fabrication of a carbon-fiber reinforced composite flat part with a recessed edge. The RTM mould comprises a rectangular cavity with dimensions 900 mm × 330 mm × 3.3 mm with a rectangular recess with dimensions 400 mm × 165 mm × 3.3 mm as illustrated in Figure 1. The sides of the cavity are sealed with silicone rubber, whilst a glass plate is placed as the top mould plate enabling visual monitoring of the flow front to be carried out. The preform comprised nine fabric plies in a $([0F/90F]_2/0F/[90F/0F]_2)$ layup of a 5H satin

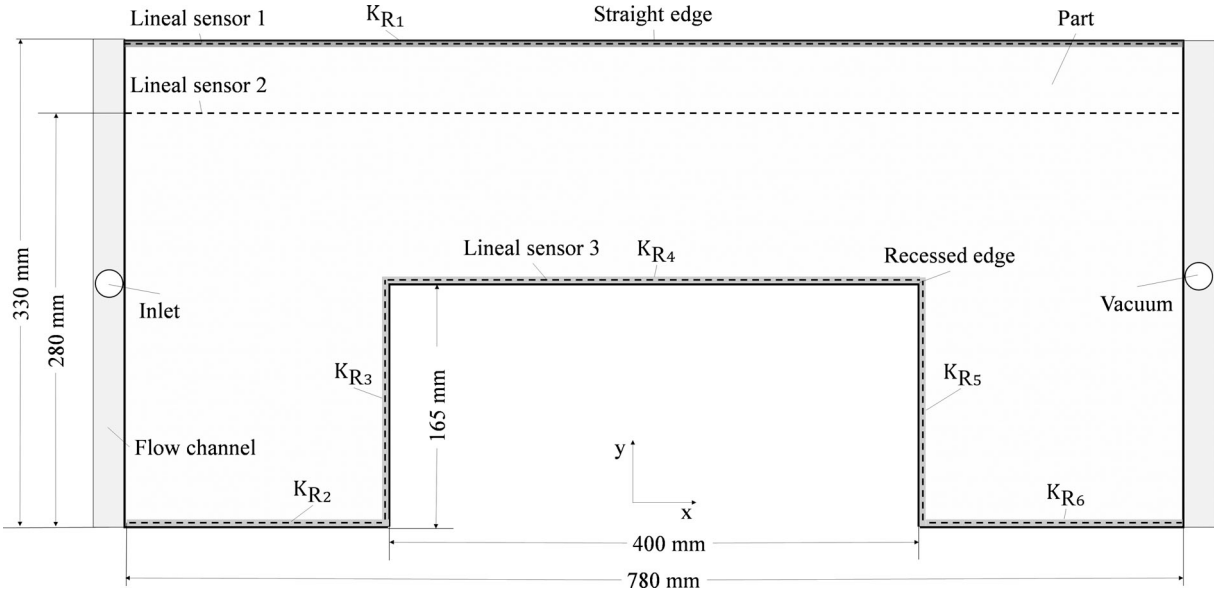

FIGURE 1 Schematic representation of the filling setup and of flow sensors positions

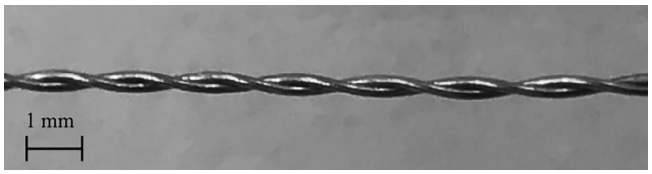

FIGURE 2 Lineal flow sensor

weave woven carbon fabric (Hexcel HexForce G0926)[24] with areal density of 375 g/m^2, resulting in a volume fraction of 57%. The matrix was Hexcel HexFlow RTM6 epoxy resin.[24] The filling process was carried out using one circular port with a rectangular flow channel resulting in linear injection initially, whilst vacuum of about 10 mbar was applied in the outlet circular port. The filling was performed in isothermal conditions at a temperature of 120°C, whilst the absolute injection pressure was 2 bar. After the completion of filling, the curing was carried out at a temperature of 160°C for 2 hours. Lineal dielectric sensors were embedded in strategic positions in the mould cavity for the monitoring of flow front evolution during the impregnation stage. The sensor type, illustrated in Figure 2, comprises two uniformly twisted copper wires insulated with polyurethane enamel and is capable of monitoring the flow front position in LCM of carbon reinforced composites.[25] The measurement area of the sensor is divided into two parts: the wetted area impregnated by resin, which fills the gaps between the wires, and the dry area in which the gaps are filled with air. As the flow process progresses the wetted area percentage increases, whilst the dry area decreases. The very large contrast in dielectric properties between liquid resin and air results in significant sensitivity of the sensor response to its covered length. The sensor can be placed either on the tool surface in contact with the carbon fabric or between two layers of reinforcement. Three sensors were utilized in this study placed on the lower surface of the mould cavity as illustrated in Figure 1. Two sensors were placed across the straight and recessed edges of the mould respectively to monitor potential racetracking effects, whilst one sensor was placed in the main flow path along the filling evolution in the main rectangle of the geometry. Thin coaxial cables passed through the outlet port were utilized to connect the sensors with a Solartron 1260 Impedance Analyzer. A Keithley 7001 switch system was used as a multiplexer between the sensors and the analyzer to allow the data acquisition for the three sensors in the same experiment. Impedance data were acquired in a sweep comprising three frequencies: 10, 31.6 and 100 KHz. The analyzer communicates with a computer via an IEEE interface and an in-house LabVIEW code was utilized to acquire impedance data. A digital camera was used for the visual monitoring of flow front position to compare the actual flow front with inverse scheme results.

2.2 | Flow modeling

The filling stage of composite manufacture can be modeled using Darcy's law expressing the viscous flow of a liquid through porous media as follows:

$$\mathbf{v_{fl}} = -\frac{\boldsymbol{\kappa}\nabla \mathbf{P}}{\eta}. \quad (1)$$

where $\mathbf{v_{fl}}$ is the Darcy velocity, $\boldsymbol{\kappa}$ the permeability tensor, η resin viscosity and **P** the pressure. The resin velocity is driven by the applied pressure gradient and is affected by material properties such as resin viscosity and preform permeability. Liquid resin is considered as incompressible, and thus in order to preserve the balance of resin mass the divergence of the flow velocity is expressed as follows:

$$\nabla \mathbf{v_{fl}} = 0 \quad (2)$$

A flow simulation model was implemented in the Control Volume/Finite Element (CV/FE) analysis solver PAM-RTM to represent the filling of the part. PAM-RTM solves Darcy's equation using non-conforming elements, whilst the flow progression is computed with the volume of fluid (VOF) method. Considering the small thickness compared to in plane dimensions, through thickness flow was assumed to be negligible and the problem was solved using membrane elements. The model comprises 5700 three noded linear membrane elements. The boundary conditions were a prescribed injection pressure of 2 bar applied in the inlet flow channel and vacuum applied on the outlet port. A constant temperature of 120°C was applied to all nodes representing isothermal filling.

The model was divided into seven zones with different permeabilities values; one representing the main flow in the preform and the other six the flow across the part edges. An equivalent permeability K_{Ri} value was assigned on each of the six edges, as shown in Figure 1, allowing the model to estimate potential racetracking effects.[26] In the case of the main flow zone, the principal permeability values K_1 and K_2 were aligned to the length and width direction respectively. Nominal values of principal permeabilities for the fabric of this study are reported in Table 1.[27]

User defined subroutines in C++ were used to represent resin viscosity evolution with temperature and time. The viscosity model utilises a reference viscosity (η_{ref}) at a temperature (T_{ref}) as a state variable.[28] The reference viscosity follows its own kinetics which can be expressed as follows:

$$\frac{d}{dt}(\ln(\eta_{ref})) = Ae^{-\frac{E}{RT}}\left(\ln\frac{\eta_{ref}}{\gamma}\right)^m \quad (3)$$

The rate of change of the reference viscosity follows an Arrhenius dependence on temperature T, where A is the preexponential factor, E the activation energy and R the universal gas constant. The rate of change of the logarithm of reference viscosity follows an autocatalytic behavior with m denoting the order and γ a coefficient. The viscosity is estimated using the reference viscosity calculated by the integration of Equation (3), as follows:

$$\eta = \eta_{ref} Ae^{-D\left(\frac{1}{T}-\frac{1}{T_{ref}}\right)} \quad (4)$$

where D is the temperature dependence coefficient. Table 1 reports viscosity model parameter values of Equations (3) and (4).[10] Uncertainty quantification experiments have shown that the initial reference viscosity ($\eta_0 = \eta_{ref}$) presents variability due to storage conditions.[10] Therefore, it was considered a stochastic variable.

TABLE 1 Nominal principal permeability values[27] and viscosity model parameters[10]

Parameter	Values	Units
Principal permeability in *x* direction: K_1	1.7×10^{-11}	m^2
Principal permeability in *y* direction: K_2	1.3×10^{-11}	m^2
Initial reference viscosity: η_0	0.17	Pas
Preexponential factor: A	370 386	s^{-1}
Activation energy: E	70 309	J/mol
Autocatalytic order: m	1.34	-
Temperature dependence coefficient: D	6800	K^{-1}
Coefficient: γ	0.39	Pas
Reference temperature: T_{Ref}	353	K

2.3 | Surrogate model

Flow process simulation using numerical solution requires moderate computational time. However, inverse schemes such as the MCMC operate in an iterative manner requiring a large number of flow model realisations making the utilisation of the simulation computational cumbersome. Surrogate models based on Kriging were constructed to overcome computational time issues by substituting the CV/FE solution. Kriging enables the unbiased prediction of untried parameter values to be made with minimum variance and more accurately in comparison with low order polynomial expansion models.[29] Figure 3 summarizes the methodology for the construction of the surrogate models. Kriging requires an initial set of input sample points at which the responses are known. Latin Hypercube

Sampling[30] was used for generating the initial input points and the flow model was utilized to compute the response at these points.

Four surrogate models were constructed for the implementation of the inversion procedure. Three of them represent the covered length S_1, S_2, and S_3 of the three sensors as function of the stochastic variables and time t. The fourth surrogate model represents the filling duration (t_{fill}) as a function of the unknown stochastic parameters. The unknown stochastic parameters are the principal permeabilities K_1 and K_2, the equivalent edge permeabilities K_{R1}-K_{R6} representing racetracking and the initial reference viscosity η_0. Preform permeability variability was represented as a scalar variable rather than a random field with autocorrelation structure.[11] This simplified approach does not consider the variations of preform permeability in local scale and spatial correlation; however, it results in a significant reduction of flow models dimensions enabling the construction of efficient surrogate models. The statistical properties of the initial reference viscosity[10] and principal permeabilities[9] are reported in Table 2. Racetracking can be characterized by racetracking strength, which is the ratio of equivalent racetracking permeability over principal permeability.[31] The RTM mould is sealed with silicone rubber along the edges, which may cause compaction to the preform edges after closing the mould. This effect was represented by a lower limit of 0.5 in racetracking strength. Conversely, inaccuracies in fabric cutting or fabric misplacement may result in a small gap between the reinforcement and the seal, which results in increasing the local permeability in the longitudinal direction of the gap. This potential effect was represented by adopting a maximum value of racetracking strength of 10. The equivalent permeability range and the statistical properties, which are reported Table 2, were calculated considering these upper and lower limits of racetracking strength.

The resulting high dimensional input space of the surrogate models requires a very large initial set of sampling points to ensure model accuracy compared to the PAM-RTM model. A sensitivity analysis was carried out in order to reduce model dimensionality investigating model response by altering each parameter by two positive and two negative SDs about their mean values. The initial reference viscosity affects the response of all sensors given the global role of viscosity in the evolution of filling. In contrast, principal and race tracking permeabilities can have a local role and only affect significantly some of the sensors responses. Therefore, only the principal and equivalent racetracking permeabilities were considered in the sensitivity analysis. The values of these parameters used in the analysis are reported in Table 3.

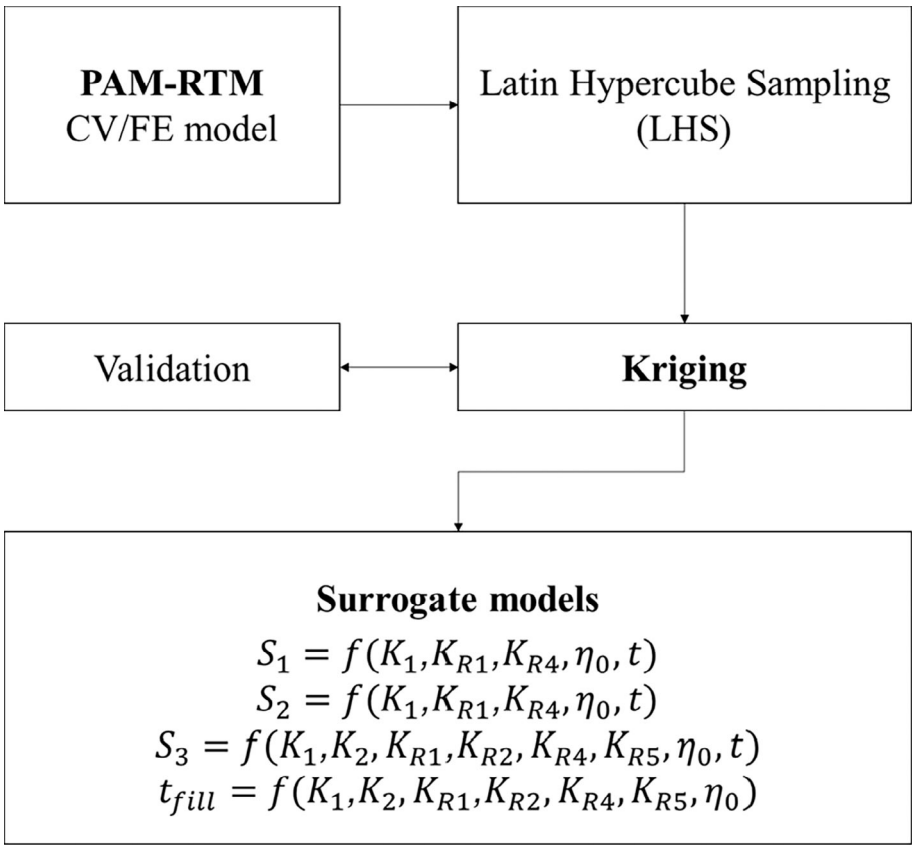

FIGURE 3 Surrogate model construction methodology

The PAM-RTM model was utilized for the evaluation of the filling for the 256 input parameters combinations. The average absolute relative difference of covered sensor length was computed for each of the input parameters as the average difference over all corresponding cases with the upper and lower value of the specific parameter. Table 3 summarizes the results of the sensitivity analysis. An absolute relative difference of 10% in sensor response was considered as the threshold beyond which the sensor is considered sensitive to the corresponding parameter. Sensors S_1 and S_2 are sensitive only to K_1, K_{R1} and K_{R4}, whereas S_3 to K_1, K_2, K_{R2}, K_{R4}, and K_{R5}. The equivalent permeability K_{R3} does not affect significantly the response of any sensor since the flow front at that area is dominated by the principal permeability K_1 and resin viscosity. In the case of K_{R6} the flow at this last edge of the part is governed by K_2 and resin viscosity due to the presence of the recessed edge. Table 4 presents the parameters of each of the surrogate models and their corresponding ranges.

Kriging expresses the covered length of sensors and filling duration as a vector $\boldsymbol{Y} = (S_1, S_2, S_3, t_{fill}) \in \mathbb{R}^4$, which is a function of input vectors $\boldsymbol{x_1} = (K_1, K_{R1}, K_{R4}, \eta_0, t) \in \mathbb{R}^5$, $\boldsymbol{x_2} = (K_1, K_{R1}, K_{R4}, \eta_0, t) \in \mathbb{R}^5$, $\boldsymbol{x_3} = (K_1, K_2, K_{R1}, K_{R2}, K_{R4}, K_{R5}, \eta_0, t) \in \mathbb{R}^8$ and $\boldsymbol{x_4} = (K_1, K_2, K_{R1}, K_{R2}, K_{R4}, K_{R5}, \eta_0) \in \mathbb{R}^7$ as follows:

$$\boldsymbol{Y}(\boldsymbol{x_i}) = \boldsymbol{f_i}(\boldsymbol{x_i})^T\boldsymbol{\beta_i} + \boldsymbol{r_i}(\boldsymbol{x_i})^T\boldsymbol{\gamma_i},\ \boldsymbol{i} = \boldsymbol{1},\ldots,\boldsymbol{4}. \tag{5}$$

where $Y(\boldsymbol{x_i}) = Y_i$. Equation (5) is a combination of a second order regression and a correlation model using a Gaussian function $\boldsymbol{f_i}(\boldsymbol{x_i})^T\boldsymbol{\beta_i}$ and $\boldsymbol{r_i}(\boldsymbol{x_i})^T\boldsymbol{\gamma_i}$ respectively following the formulation described in.[32] The regression model expresses the output variable as a linear combination of p basis functions $\boldsymbol{f_i}(\boldsymbol{x_i}) : \mathbb{R}^p \rightarrow \mathbb{R}$, whilst $\boldsymbol{\beta} \in \mathbb{R}^p$ is the vector of regression parameters computed using generalized least squares.[32] Term $\mathbf{r_i}(\boldsymbol{x_i})$ in correlation model corresponds to a vector of cross-correlations between input point $\boldsymbol{x_i}$ and each of N sampling points ($\boldsymbol{s_{x_i}} \in \mathbb{R}^{n_i}$). Vector $\boldsymbol{\gamma}^* \in \mathbb{R}^{\mathbf{N}}$ is computed as follows:

$$\boldsymbol{\gamma}^* = \boldsymbol{\mathcal{R}}^{-1}\begin{pmatrix} \boldsymbol{s_y^1} - \boldsymbol{f}\left(\boldsymbol{s_x^1}\right)^T\boldsymbol{\beta} \\ \vdots \\ \boldsymbol{s_y^N} - \boldsymbol{f}\left(\boldsymbol{s_x^N}\right)^T\boldsymbol{\beta} \end{pmatrix}. \tag{6}$$

where $\boldsymbol{\mathcal{R}} \in \mathbb{R}^{N \times N}$ denotes the correlation matrix of all sampling points and $s^1_{y_i},\ldots,s^N_{y_i}$ the responses at sampling points $\boldsymbol{s^1_{x_i}},\ldots,\boldsymbol{s^N_{x_i}}$. The MATLAB toolbox was utilized for the calculation of surrogate models coefficients.[33] The predictor in Equation (5) was implemented in Visual Studio C++.

TABLE 2 Statistical properties of principal permeabilities,[9] viscosity[10] and equivalent racetracking permeability

Parameter	Average	SD
Principal permeability: $K_1(m^2)$	1.7×10^{-11}	3.4×10^{-12}
Principal permeability: K_2 (m^2)	1.3×10^{-11}	2.6×10^{-12}
Racetracking permeability: K_{Ri} (m^2)	4×10^{-11}	1.5×10^{-11}
Initial reference viscosity: η_0 (Pas)	0.17	0.8

2.4 | Inverse algorithm

An inverse scheme was developed for the real time uncertainty estimation of the unknown stochastic parameters and the filling duration. Figure 4 summarizes the

TABLE 3 Sensitivity analysis parameter values and results

			Average relative difference		
Parameter	Lower value	Upper value	Sensor 1	Sensor 2	Sensor 3
Principal permeability: K_1 (m^2)	1×10^{-11}	2.4×10^{-11}	**38%**	**41%**	**40%**
Principal permeability: K_2 (m^2)	9×10^{-12}	1.9×10^{-11}	3%	2%	**22%**
Racetracking permeability: K_{R1} (m^2)	1×10^{-11}	7×10^{-11}	**44%**	**28%**	**14%**
Racetracking permeability: K_{R2} (m^2)	1×10^{-11}	7×10^{-11}	2%	2%	**65%**
Racetracking permeability: K_{R3} (m^2)	1×10^{-11}	7×10^{-11}	3%	3%	3%
Racetracking permeability: K_{R4} (m^2)	1×10^{-11}	7×10^{-11}	**8%**	**9%**	**30%**
Racetracking permeability: K_{R5} (m^2)	1×10^{-11}	7×10^{-11}	1%	1%	**20%**
Racetracking permeability: K_{R6} (m^2)	1×10^{-11}	7×10^{-11}	0.04%	0.05%	4%

Note. Bold values denote cases for which the sensitivity is considered significancy.

TABLE 4 Surrogate models parameters and their ranges

Parameter	Range	S_1	S_2	S_3	t_{fill}
Principal permeability: K_1 (m^2)	5×10^{-12} - 2×10^{-11}	Yes	Yes	Yes	Yes
Principal permeability: K_2 (m^2)	5×10^{-12} - 2×10^{-11}	No	No	Yes	Yes
Racetracking permeability: K_{R1} (m^2)	5×10^{-12} - 1×10^{-10}	Yes	Yes	Yes	Yes
Racetracking permeability: K_{R2} (m^2)	5×10^{-12} - 1×10^{-10}	No	No	Yes	Yes
Racetracking permeability: K_{R4} (m^2)	5×10^{-12} - 1×10^{-10}	Yes	Yes	Yes	Yes
Racetracking permeability: K_{R5} (m^2)	5×10^{-12} - 1×10^{-10}	No	No	Yes	Yes
Initial reference viscosity: η_0 (Pas)	0.11-0.22	Yes	Yes	Yes	Yes

Note. Yes: Significant and No: Not significant.

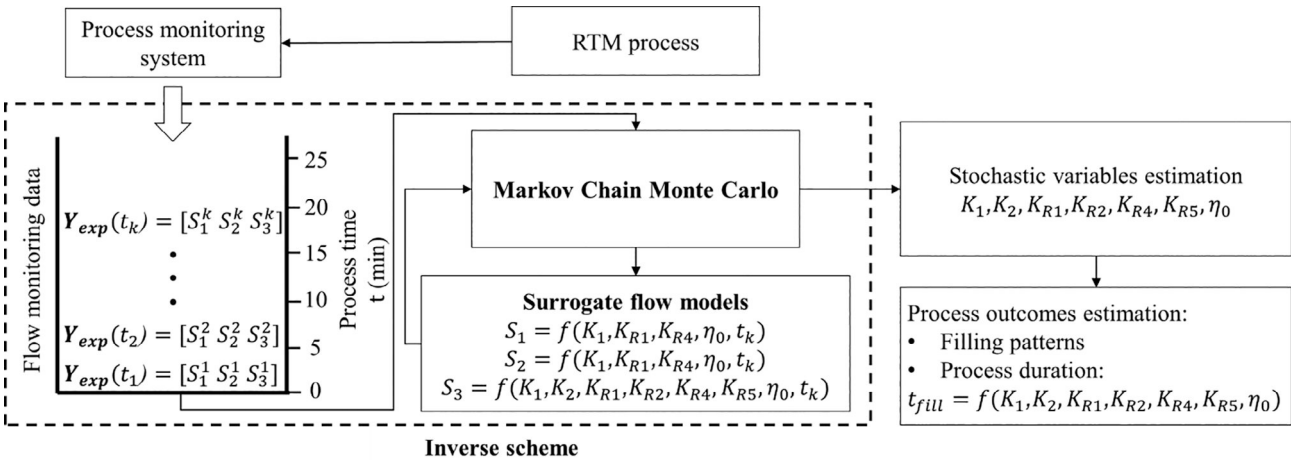

FIGURE 4 Inversion procedure framework

inversion procedure framework. The analysis is initiated when the filling stage of the RTM process takes place. The sensors monitor the covered length S_1, S_2 and S_3 at each time increment t_k. The inverse scheme integrates the monitoring data in real time with the surrogate flow models using the Markov Chain Monte Carlo (MCMC) method for the probabilistic prediction of the unknown stochastic parameters and the filling duration. MCMC operates as a sampler drawing a series of parameter realizations with a probability of acceptance proportional to the conditional incremental likelihood of process monitoring data. The accepted realizations constitute the solution of the inverse problem in the form of a probabilistic estimate of process outcomes. MCMC is based on Bayes' theorem and is utilized in many inverse problems due to its simplicity.[34–36] According to Bayes' theorem, measurements $\boldsymbol{Y}_{\mathbf{exp}}(t_k) \in \mathbb{R}^{N_k \times 3}$, with N_k the number of experimental data, which correspond to covered lengths of the three lineal sensors at times $t_1 \ldots t_k$, are connected to the corresponding surrogate model responses $\mathbf{S} = (\boldsymbol{S_1}, \boldsymbol{S_2}, \boldsymbol{S_3}) \in \mathbb{R}^{N_k \times 3}$ as follows:

$$\boldsymbol{P}(\boldsymbol{S}|\boldsymbol{Y}_{\mathbf{exp}}) \propto \boldsymbol{P}(\boldsymbol{Y}_{\mathbf{exp}}|\boldsymbol{S})\boldsymbol{P}(\boldsymbol{S}). \quad (7)$$

where $P(\boldsymbol{S}|\ \boldsymbol{Y}_{\mathbf{exp}})$ denotes the posterior probability, $P(\boldsymbol{Y}_{\mathbf{exp}}|\ \boldsymbol{S})$ the likelihood distribution and $P(\boldsymbol{S})$ the prior distribution. Equation (7) expresses the probability of model response $\boldsymbol{S}_{\mathbf{i\ =\ 1,2,3}}(\boldsymbol{V}, t_k)$ for a given set of unknown stochastic parameters $\boldsymbol{V}$ conditional to flow monitoring data $\boldsymbol{Y}_{\mathbf{exp}}(t_k)$. MCMC utilises Bayes' theorem to accept or reject the proposed set of input samples, which in this case are the unknown stochastic parameters. The random walk Metropolis Hastings algorithm was utilized to generate samples $\boldsymbol{V}_{\mathbf{j}} = [K_1\ K_2\ K_{R1}\ K_{R2}\ K_{R4}\ K_{R5}\ \eta_0] \in \mathbb{R}^7$, where subscript j denotes the current MCMC iteration, from a symmetric normal proposal distribution $q(\boldsymbol{V}_{\mathbf{j}}|\ \boldsymbol{V}_{\mathbf{j\ -\ 1}})$ resulting in a simplified draw of new samples. Due to the symmetry the new sample $\boldsymbol{V}_{\mathbf{j}}$ is calculated using an incremental step drawn from the multivariate Gaussian variable $\boldsymbol{\varepsilon} = (\varepsilon_{K_1}\ \varepsilon_{K_2}\ \varepsilon_{K_{R1}}\ \varepsilon_{K_{R2}}\ \varepsilon_{K_{R4}}\ \varepsilon_{K_{R5}}\ \varepsilon_{\eta_0}) \in \mathbb{R}^7$ with mean value 0 and SD $\boldsymbol{\sigma}_{\boldsymbol{\varepsilon}} = \left(\sigma_{\varepsilon_{K_1}} \sigma_{\varepsilon_{K_2}} \sigma_{\varepsilon_{K_{R1}}}\ \sigma_{\varepsilon_{K_{R2}}} \sigma_{\varepsilon_{K_{R4}}} \sigma_{\varepsilon_{K_{R5}}} \sigma_{\varepsilon_{\eta_0}}\right) \in \mathbb{R}^7$, applied to sample $\boldsymbol{V}_{\mathbf{j-1}}$ from the previous step. An acceptance criterion is applied to each of the samples generated and by accepting or rejecting it the posterior probability

TABLE 5 Metropolis hastings algorithm

Algorithm 1 Metropolis Hastings algorithm

Initialize $\boldsymbol{V_0} = (K_{10}\ K_{20}\ K_{R10}\ K_{R20}\ K_{R40}\ K_{R50}\ \eta_{00})$
for $j = 1$ to M
  Draw a sample u~U(0, 1) from a uniform distribution.
  Draw sample $\boldsymbol{\varepsilon}\sim N(\boldsymbol{0}, \boldsymbol{\sigma_\varepsilon}) \longrightarrow \boldsymbol{V_j = V_{j-1} + \varepsilon}$
  Calculate acceptance probability

$$\alpha = \min\left\{1, \frac{P\left(\boldsymbol{Y_{exp}}(t)|\boldsymbol{S_i}\left(\boldsymbol{V_j}, t\right)\right)P\left(\boldsymbol{V_j}\right)}{P\left(\boldsymbol{Y_{exp}}(t)|\boldsymbol{S_i}\left(\boldsymbol{V_{j-1}}, t\right)\right)P\left(\boldsymbol{V_{j-1}}\right)}\right\}$$

  if $u \le \alpha$ then
    accept $\boldsymbol{V_j}$
  else
    $\boldsymbol{V_j} = \boldsymbol{V_{j-1}}$
  end if
end for

Note. Bold variables denote vectors following the notation of the manuscript.

converges to the target distribution $P(\boldsymbol{S_i}(\boldsymbol{V}, t)|\ \boldsymbol{Y_{exp}}(t))$. The algorithm operates as shown in Table 5 and the procedure is repeated M times, where M is the number of the MCMC iterations.

The likelihood distribution is expressed as:

$$P\left(\boldsymbol{Y_{exp}}(t)|\boldsymbol{Y_m}\left(\boldsymbol{V_j}, t\right)\right) = \prod_{k=1}^{N_k} N\left(\boldsymbol{Y_{exp}}(t_k); \boldsymbol{S_i}\left(\boldsymbol{V_j}, t_k\right), \sigma\right). \tag{8}$$

where N_k denotes the total number of experimental data acquired by the time t_k. The likelihood incorporates all the distributions, which are computed with experimental data $\boldsymbol{Y_{exp}}(t_k)$ using a normal distribution with the model values $\boldsymbol{S_i}(\boldsymbol{V_j}, t_k)$ as a mean and a SD σ.

The prior distribution is computed in a similar way for the three sensor surrogate models:

$$P\left(\boldsymbol{V_j}\right) = \prod_{l=1}^{7} N\left(V_j^l; \mu_{prior}^l, \sigma_{prior}^l\right). \tag{9}$$

The statistical properties of prior distributions of the unknown parameters are:

$$\begin{aligned}\boldsymbol{\mu_{prior}} &= \left(\mu_{prior}^{K_1}\ \mu_{prior}^{K_2}\ \mu_{prior}^{K_{R1}}\ \mu_{prior}^{K_{R2}}\ \mu_{prior}^{K_{R4}}\ \mu_{prior}^{K_{R5}}\ \mu_{prior}^{\eta_0}\right) \in \mathbb{R}^7 \\ \boldsymbol{\sigma_{prior}} &= \left(\sigma_{prior}^{K_1}\ \sigma_{prior}^{K_2}\ \sigma_{prior}^{K_{R1}}\ \sigma_{prior}^{K_{R2}}\ \sigma_{prior}^{K_{R4}}\ \sigma_{prior}^{K_{R5}}\ \sigma_{prior}^{\eta_0}\right) \in \mathbb{R}^7\end{aligned}. \tag{10}$$

with values based on uncertainty quantification of previous studies, which are summarized in Table 2.

TABLE 6 Inverse scheme parameters values

Parameter	Symbol	Value
Likelihood distribution SD	σ	10 mm
Noise level ε_{K_1} SD	$\sigma_{\varepsilon_{K_1}}$	3×10^{-13} m^2
Noise level ε_{K_2} SD	$\sigma_{\varepsilon_{K_2}}$	3×10^{-13} m^2
Noise level $\varepsilon_{K_{R1}}$ SD	$\sigma_{\varepsilon_{K_{R1}}}$	3×10^{-13} m^2
Noise level $\varepsilon_{K_{R2}}$ SD	$\sigma_{\varepsilon_{K_{R2}}}$	3×10^{-13} m^2
Noise level $\varepsilon_{K_{R4}}$ SD	$\sigma_{\varepsilon_{K_{R4}}}$	3×10^{-13} m^2
Noise level $\varepsilon_{K_{R5}}$ SD	$\sigma_{\varepsilon_{K_{R5}}}$	3×10^{-13} m^2
Noise level ε_{η_0} SD	$\sigma_{\varepsilon_{\eta_0}}$	0.001 Pas
Number of MCMC iterations	M	20 000 iterations
Process duration	D	32 min
Number of monitoring data	N	96
Number of data batches	k	32

Abbreviation: MCMC, Markov Chain Monte Carlo.

SDs σ and $\boldsymbol{\sigma_\varepsilon}$ need to be adjusted before the initiation of the inversion procedure. SD σ is utilized in the likelihood distribution to express the accuracy of the experimental data and it is assigned a relative small value of 10 mm based on the evaluation of sensor error presented in.[25] The SD vector defines the size of the sampling step of the chain.[37] A short sequence of MCMC iterations was carried out at the beginning of the inverse algorithm to tune the vector of SD $\boldsymbol{\sigma_\varepsilon}$ of the algorithm targeting an acceptance probability between 30% and 50%.[37] The values of SDs are reported in Table 6. In the real time implementation of inversion procedure, the monitoring matrix $\boldsymbol{Y_{exp}}$ is updated every minute with a new batch of monitoring data. In this case every new batch includes three data points corresponding to the three sensor responses. The number M of MCMC iterations carried out in the real time implementation of the inversion procedure can be calculated based on the time of the execution of one MCMC iteration. The execution time of one iteration for a given computer increases with the increase of the size of $\boldsymbol{Y_{exp}}$. The number of MCMC iterations executed at the beginning of the process is about 2500 points/min on a high specification personal computer (4 cores @3.2 GHz), whilst this number decreases gradually to about 170 point/min in the last stage of the process. The total number of MCMC iterations was approximately 20 000.

3 | RESULTS AND DISCUSSION

3.1 | Surrogate model validation

Surrogate models representing flow front position of each sensor and filling duration were evaluated against the

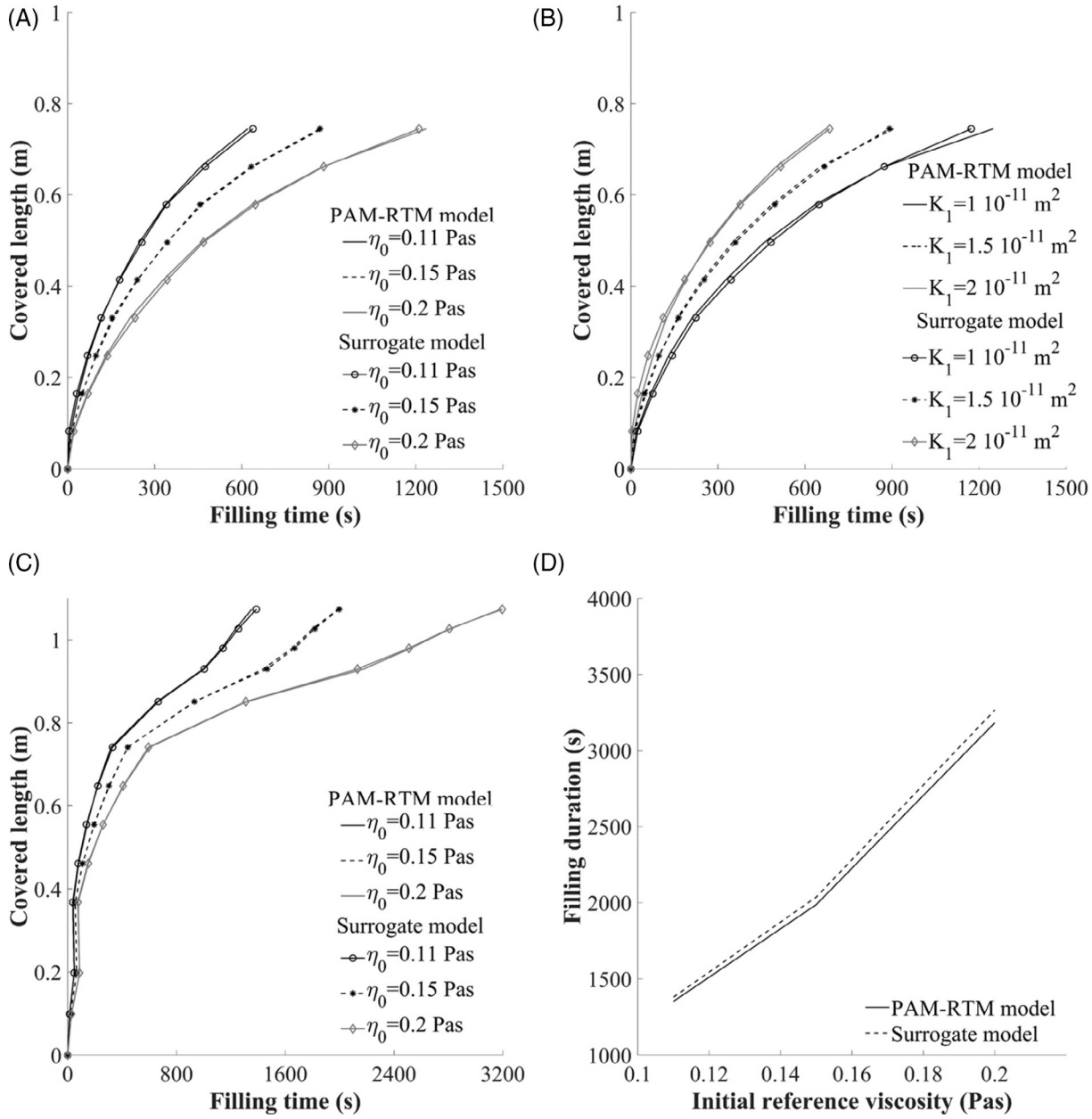

FIGURE 5 Surrogate model validation against the CV/FE simulation: A, sensor 1, B, sensor 2, C sensor 3, and D, filling duration. CV/FE, control volume/finite element

TABLE 7 Input parameters values used for the construction of validation curves (Figure 5)

Parameter	Sensor 1 (S_1)	Sensor 2 (S_2)	Sensor 3 (S_3)	Filling duration (t_{fill})
Principal permeability: K_1 (m^2)	1.7×10^{-11}	**1×10^{-11} -2×10^{-11}**	1.7×10^{-11}	1.7×10^{-11}
Principal permeability: K_2 (m^2)	–	–	1.3×10^{-11}	1.3×10^{-11}
Racetracking permeability: K_{R1} (m^2)	1.3×10^{-11}	1.3×10^{-11}	1.3×10^{-11}	1.3×10^{-11}
Racetracking permeability: K_{R2} (m^2)	–	–	1.3×10^{-11}	1.3×10^{-11}
Racetracking permeability: K_{R4} (m^2)	1.3×10^{-11}	1.3×10^{-11}	1.3×10^{-11}	1.3×10^{-11}
Racetracking permeability: K_{R5} (m^2)	–	–	1.3×10^{-11}	1.3×10^{-11}
Initial reference viscosity: η_0 (Pas)	**0.1-0.2**	0.15	**0.1-0.2**	**0.11–0.2**

Note. Bold values denote ranges of variables.

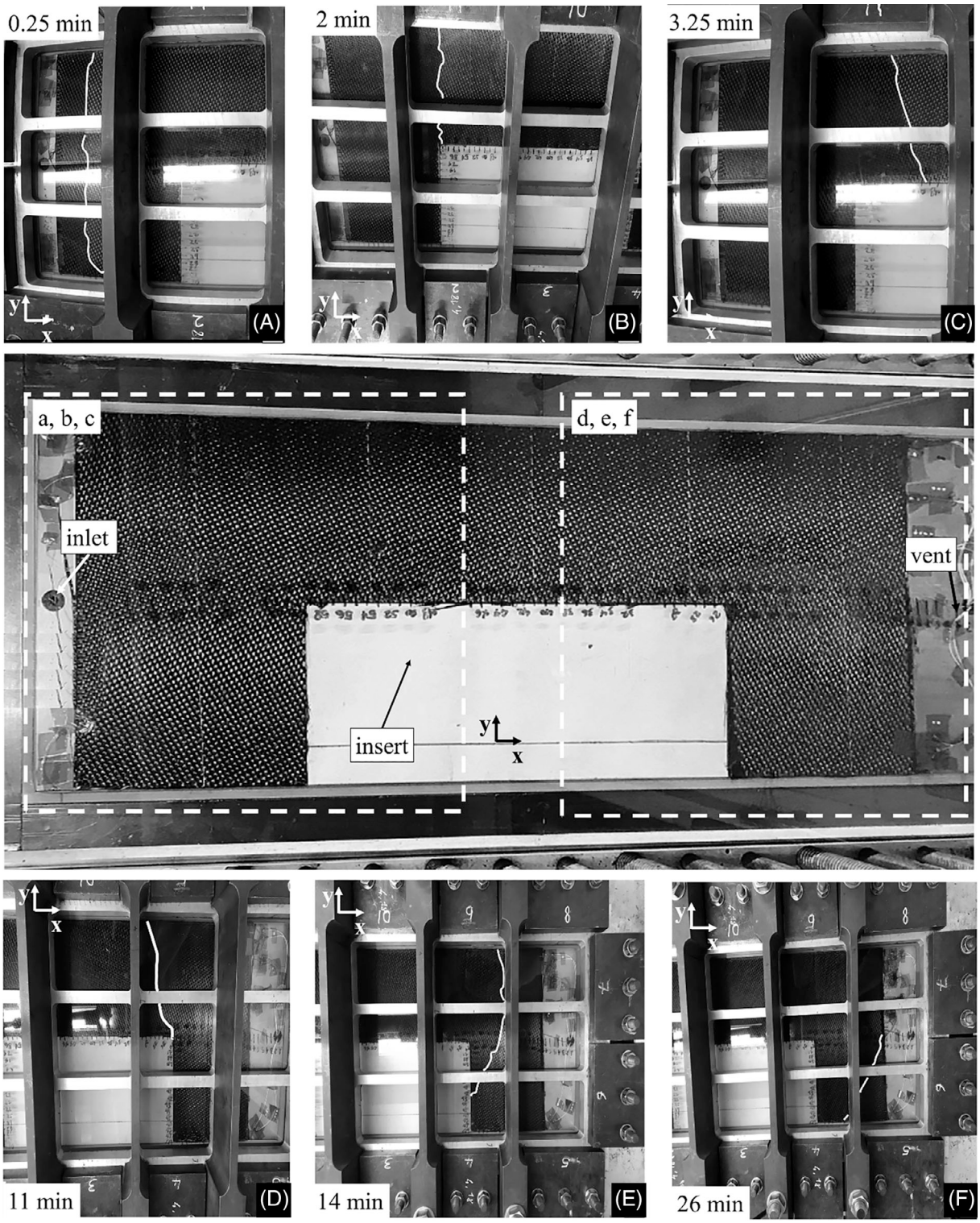

FIGURE 6 Flow front position during RTM process. RTM, resin transfer molding

PAM-RTM flow model. Validation for the surrogate models was carried out based on comparisons between the surrogate model and simulation with varying input parameters values. Three different cases were tested for the surrogate models, which express sensor response. The surrogate model of S_1 was compared with the simulation for three different initial reference viscosity values with the longitudinal principal permeabilities K_1 and K_2 equal to 1.7×10^{-11} and 1.3×10^{-11} m^2 respectively and racetracking permeabilities K_{R1} K_{R2} and K_{R4} of 1.3×10^{-11} m^2. The results are illustrated in Figure 5A. The estimated flow front position of S_1 is in good

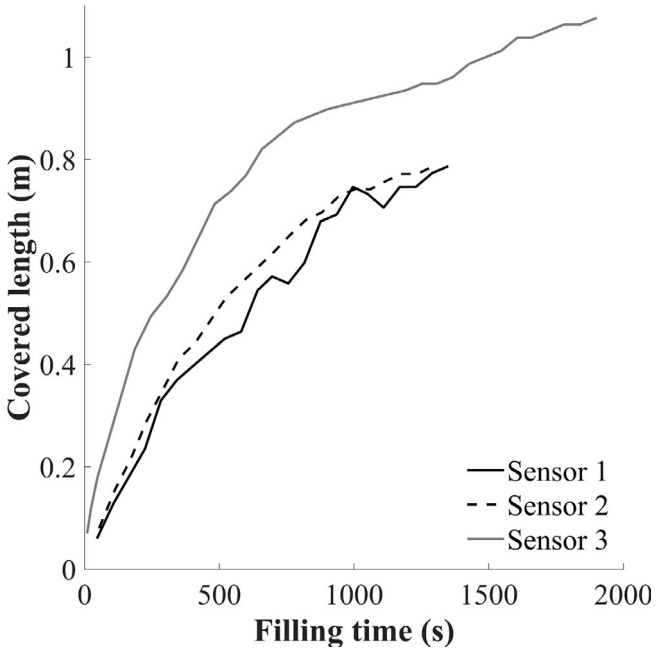

FIGURE 7 Flow monitoring results

agreement with the corresponding PAM-RTM model results and reproduces trends of dependence on viscosity correctly. Figure 5B depicts the evolution of flow front position of the second sensor (S_2) for three different longitudinal principal permeability values with the transverse principal permeability equal to 1.3×10^{-11} m^2, racetracking permeabilities K_{R1}, and K_{R4} 1.3×10^{-11} m^2 and initial reference viscosity 0.15 Pas as computed by the surrogate and PAM-RTM models. The discrepancies between the two models are negligible with the average absolute error of about 15 mm. The response of the surrogate model of Sensor 3 corresponds to a total covered length greater than the other two models as this sensor covers the recessed edge of the part. Figure 5C illustrates S_3 for three different initial reference viscosity values with the principal permeabilities K_1 and K_2 equal to 1.7×10^{-11} and 1.3×10^{-11} m^2 respectively and racetracking permeabilities K_{R1}, K_{R2}, K_{R4} and K_{R5} of 1.3×10^{-11} m^2 as estimated by the two models. The average absolute error of surrogate model is about 12 mm highlighting the accuracy of the surrogate model. Figure 5D illustrates the comparison between the filling duration surrogate model and the PAM-RTM solution for different initial viscosity values with the principal permeabilities K_1 and K_2 equal to 1.7×10^{-11} and 1.3×10^{-11} m^2 respectively and racetracking permeabilities K_{R1}, K_{R2}, K_{R4}, and K_{R5} 1.3×10^{-11} m^2. The estimated average absolute error is about 50 seconds or less than 2% of the filling duration estimated using the simulation. The input parameters and the ranges of the validation cases are reported in Table 7.

3.2 | Filling results

The flow front evolution of the filling stage of the RTM process is presented in Figure 6. The duration of the filling was 32 minutes. Racetracking occurs at the recessed edge at the beginning of the process. In the straight edge, the flow is slightly slower than the main flow due to local compaction by the silicone rubber. The presence of the rectangular insert results in asymmetric flow in which the resin fills the straight edge of the part first and then the area close to the recessed edge. Figure 7 illustrates the flow monitoring results of the three lineal flow sensors. The flow front evolution of the first sensor (S_1) presents some disturbances potentially due to measurement noise effects or the presence of local reinforcement variations leading to non-uniform flow across the straight edge of the part. The latter can be attributed to the preparation of the preform and its placement in the mould resulting in variations of the gap size between preform and mould across the edge and in turn in variations of local edge permeability. The flow front curve of sensor 3 (S_3) indicates the different flow front velocities of each of the sub-sections of the recessed edge of the mould. At the beginning of the flow process the slope of the S_3 curve is steeper than those of S_1 and S_2 implying a racetracking effect on the recessed edge of the mould, which is also observed by visual monitoring.

3.3 | Real time uncertainty estimation

The flow monitoring data were integrated into the inverse scheme for the real time uncertainty estimation of the stochastic parameters. The inversion procedure uncertainty estimation results for the unknown stochastic parameters and the filling duration are presented in Figure 8. The use of the surrogate models allows the execution of MCMC iterations as the filling process evolves. Consequently, the results are presented as a function of filling time, which corresponds to the monitoring data and inverse estimation up to the specific point in the filling process. The estimated principal permeabilities K_1 and K_2 reach a plateau of 1.31×10^{-11} m^2 and 1.17×10^{-11} m^2 respectively after about 25 minutes from the beginning of the flow stage as depicted in Figure 8A. Both parameters present significant variations in the initial stages of the inversion due to the limited monitoring data available at that time. As the inversion proceeds, the uncertainty is narrowed down. The estimated equivalent racetracking permeabilities K_{R1}, K_{R2}, K_{R4}, and K_{R5} present similar behavior in Figure 8B. The equivalent permeability of the straight edge (K_{R1}) converges after 5 minutes as

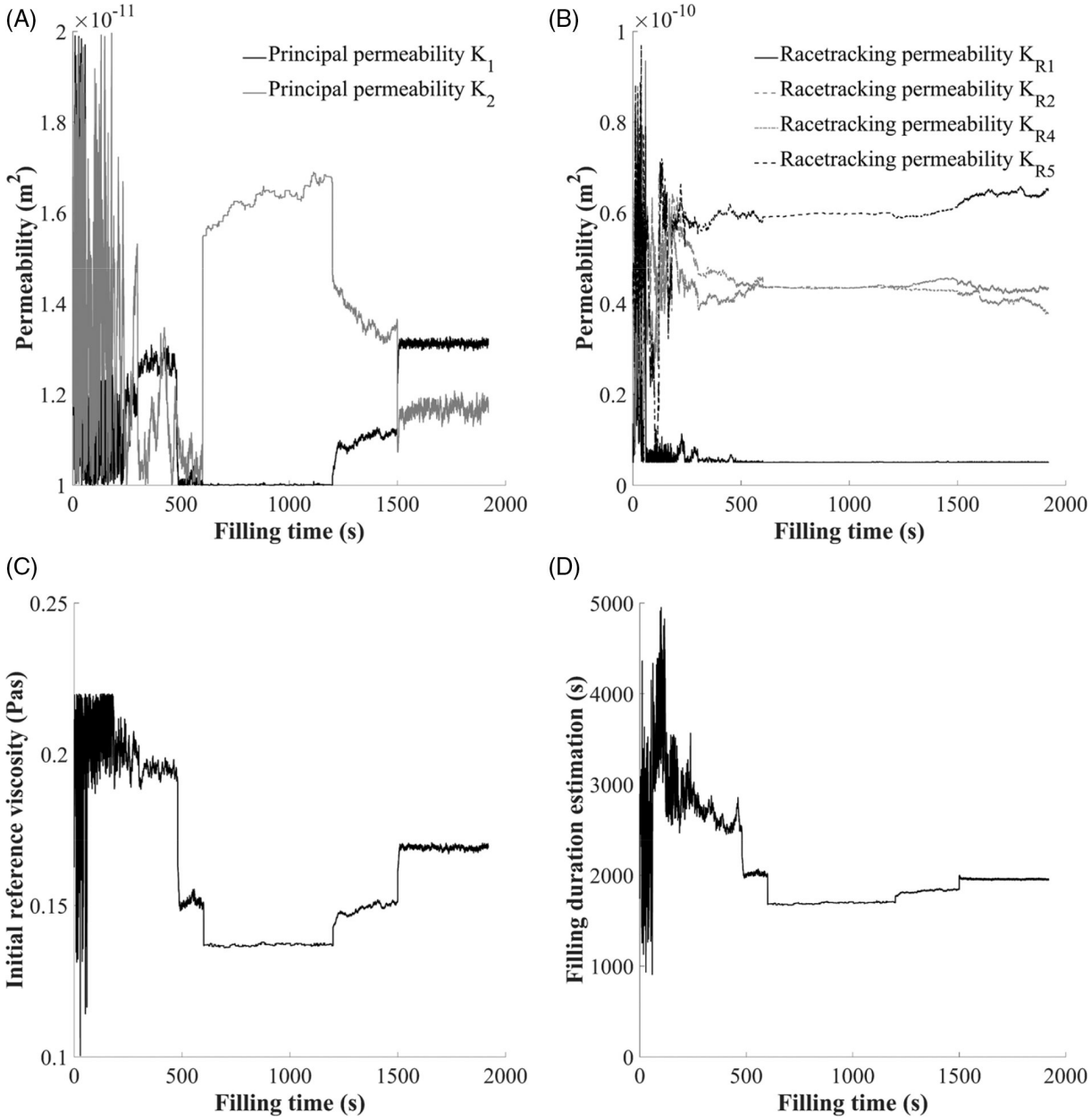

FIGURE 8 Unknown stochastic parameters estimation: A, principal permeabilities, B, equivalent racetracking permeabilities, C, initial reference viscosity, and D, filling duration estimation

TABLE 8 Statistical properties of estimated parameters

Parameter	Average	Standard deviation
K_1 (m^2)	1.312×10^{-11}	4.52×10^{-14}
K_2 (m^2)	1.168×10^{-11}	1.26×10^{-13}
K_{R1} (m^2)	5.044×10^{-12}	3.81×10^{-14}
K_{R2} (m^2)	4.056×10^{-11}	1.07×10^{-12}
K_{R4} (m^2)	4.318×10^{-11}	5.22×10^{-13}
K_{R5} (m^2)	6.422×10^{-11}	5.63×10^{-13}
η_0 (Pas)	0.1691	5×10^{-4}

the monitoring data of sensor 1 are sufficient to provide information regarding the flow front evolution in the corresponding region. The other four equivalent permeabilities (K_{R2}, K_{R4}, K_{R5}) are in the range of 4×10^{-11} to 6×10^{-11} m^2 and are mostly stabilized after about 10 minutes, highlighting the occurrence of racetracking effects in the recessed edge. The initial reference viscosity reaches a plateau of 0.17 Pas after about 25 minutes (Figure 8C). Table 8 summarizes the statistical properties of the estimated stochastic parameters. Parameters such as the longitudinal permeability,

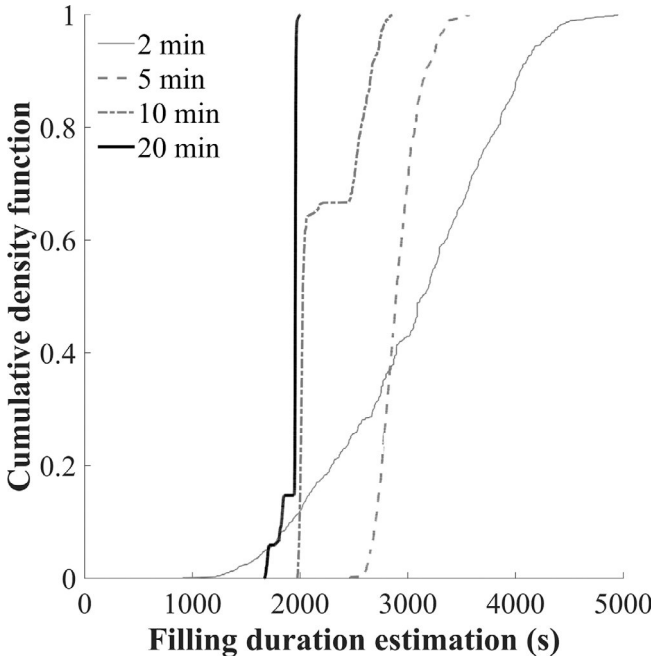

FIGURE 9 Cumulative density function evolution of estimated filling duration

the equivalent permeability of racetracking channel 1 and the initial viscosity present lower variability than the other parameters due to the greater sensitivity of the monitoring data set to these variables. It is possible to predict the duration of the filling process as well as other features of the filling process using the unknown parameter values estimated in real time by the inverse scheme. Figure 8D illustrates the estimation of filling duration as the filling stage evolves. Initially the uncertainty of filling duration estimation is significant since the available monitoring data are insufficient for an accurate prediction with low uncertainty. However, as the monitoring data are enriched, the probabilistic estimation of filling duration is narrowed down as illustrated in Figure 9. Initially the coefficient of variation of the estimated filling duration is about 25%, whilst after about 20 minutes the uncertainty is reduced by 80% to a coefficient of variation of 5%. The predicted filling duration converges to an average of 31 minutes with a SD of 1.5 minutes, whilst the actual filling takes 32 minutes. The filling duration can be estimated accurately after the completion of 10 minutes of the filling stage as can be observed in Figure 8D. In this stage, the principal permeabilities and the viscosity have not yet reached convergence, although the inverse scheme provides accurate estimation of the total filling time due to the inverse correlation of the permeability and viscosity. The convergence of the filling duration prediction occurs when the mould is 75% filled. This occurs after the flow front passes the recessed edge and thus the K_2 permeability dominates the filling pattern rather than K_1. Therefore, the flow becomes slower and data related to K_2 permeability are being fed into the inversion scheme accelerating the convergence of the filling duration.

Figure 10 illustrates the robustness of the inversion procedure in terms of reducing the uncertainty of flow front estimation. The 95% confidence intervals of the response three sensors, illustrated in Figures 10A,C,E, were calculated considering the initial uncertainty of the input parameters (Table 2). The confidence intervals of the prior estimate are wide due to the initial uncertainty of the problem, whilst the coefficient of variation of the predicted filling duration is equal to 30%. Figures 10B,D, F illustrate the 95% confidence intervals of the three sensors calculated considering the inverse solution. The confidence intervals of the estimated covered lengths have been significantly narrowed down, whilst there is a good agreement between posterior prediction and the actual covered length. The real time implementation of the inverse scheme is able to estimate the flow front evolution and filling duration with high accuracy. The discrepancies observed between model predictions and sensors data are attributed to the fact that the scheme does not consider local flow phenomena such as nesting or preform imperfections, in contrast to sensors, which are sensitive to local effects. The incorporation of local permeability into surrogate models as input variables would increase the dimensionality making the problem difficult to address with conventional computational resources. The inversion procedure gives a probabilistic estimation of the main flow parameters (ie, principal permeabilities, viscosity) and boundary conditions (ie, racetracking effects) allowing the probabilistic on line prediction of the filling duration and flow front evolution.

The flow fronts corresponding to the first and third quartiles of the prior estimate and using the outcome of the inverse scheme are illustrated in Figure 11 and compared to the actual flow front measured visually. The uncertainty obtained by the prior estimate is high as is mainly driven by the initial variability of material properties and process parameters. With the initiation of the filling process the upcoming monitoring data enhance the capabilities of the inverse scheme and thus the probabilistic estimations of the flow front present low variations and are very close to the visual observations. There are small differences between the inverse scheme estimations and the actual flow front at the beginning of process mainly due to noise effects in the experimental data and the presence of local flow phenomena. As the flow evolves, the estimated flow front follows closely the actual resin front position

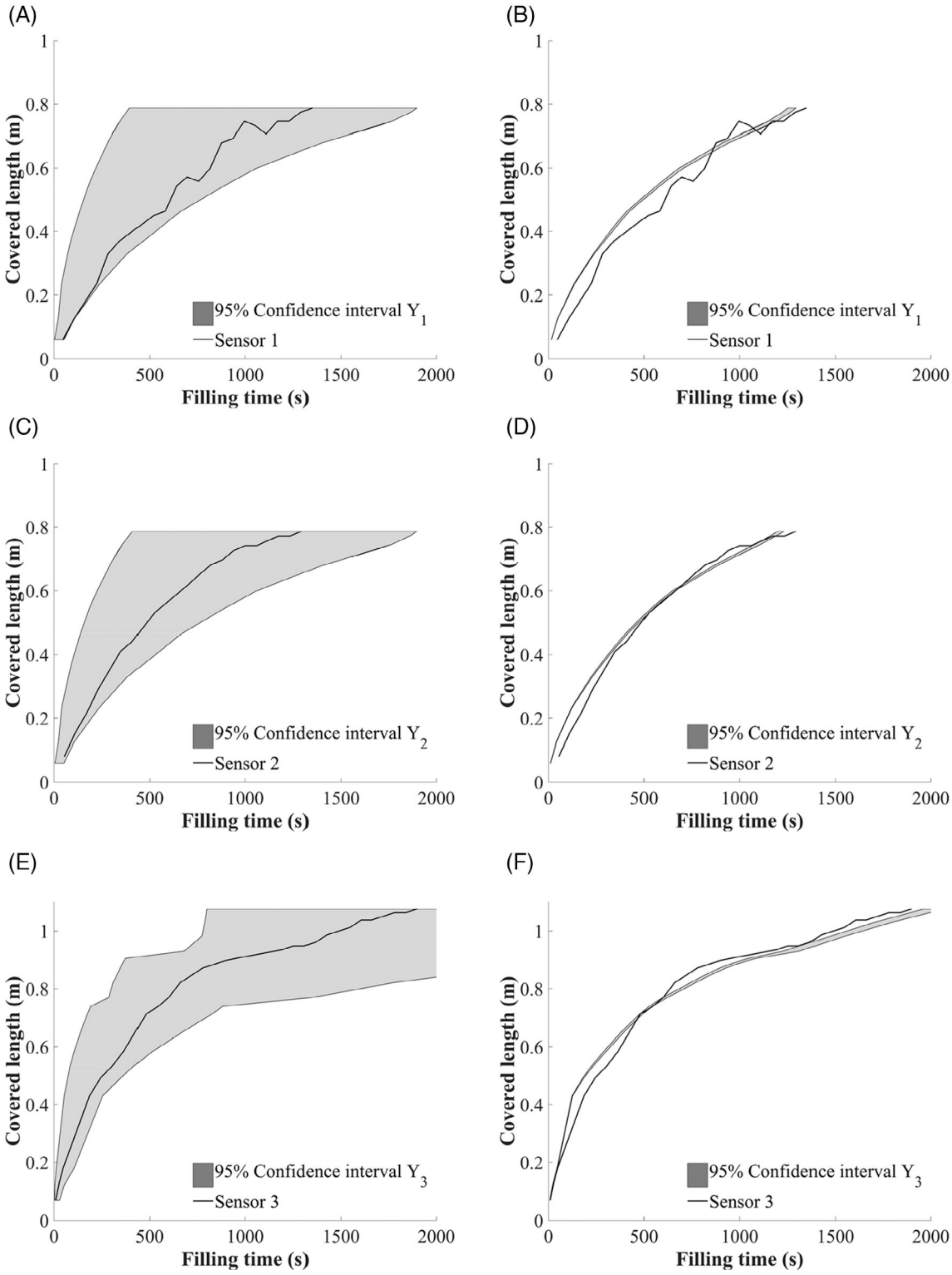

FIGURE 10 Estimation uncertainty of covered length of A, sensor 1 before the filling, B, sensor 1 after 1500 seconds, C, sensor 2 before the filling, D, sensor 2 after 1500 seconds, E, sensor 3 before the filling, and F, sensor 3 after 1500 seconds

identifying potential disturbances such as racetracking effects at the part edges.

For the geometry examined here the use of three lineal sensors in the mould is sufficient for the inverse scheme to predict accurately the resin flow front evolution and to identify potential flow disturbances and defects such as racetracking. The location of lineal sensors in the mould is crucial for the successful estimation

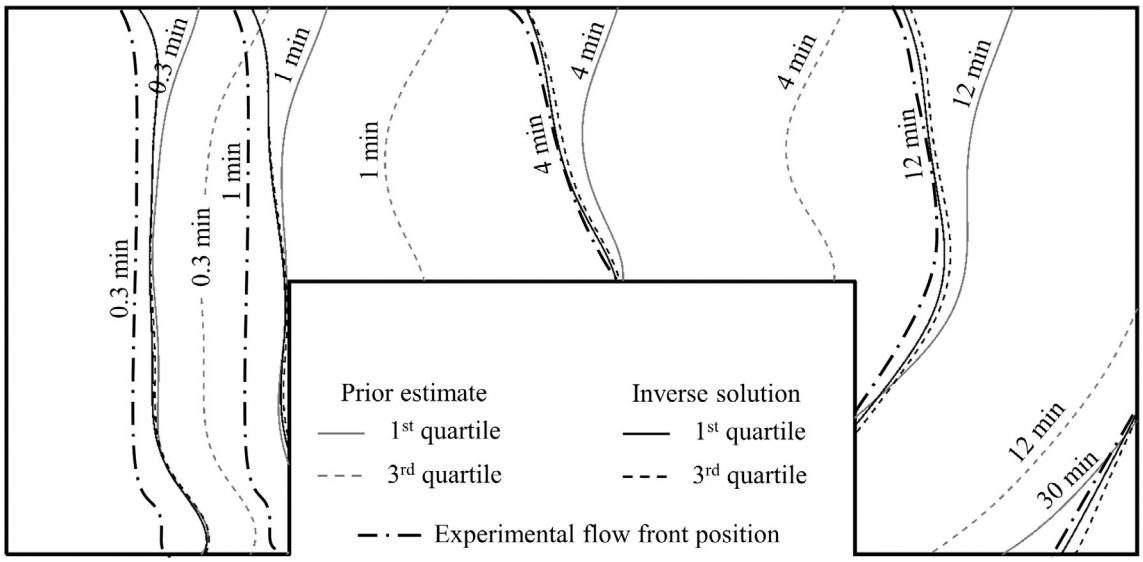

FIGURE 11 Experimental flow front and iso-probability contours at different times for prior and posterior flow front estimates

of unknown parameters. In the general case, the number of sensors used needs to be selected considering the trade-off between minimizing monitoring complexities and monitoring system intrusiveness and maximizing the sensitivity of the data obtained to all stochastic parameters of interest. In this case the utilization of three sensors placed across part edges and the main flow allows the model to capture the main process parameters such as K_1, K_2, and η_0 and provide sufficient information on racetracking phenomena.

4 | CONCLUSIONS

The inversion procedure developed in this study links real time flow monitoring data and flow modeling with the MCMC method for the probabilistic estimation of stochastic input parameters and process outcomes. The inverse scheme reduces the initial uncertainty of the problem estimating the principal permeability values, initial viscosity, racetracking effects, filling duration, and flow front evolution with significantly lower variability than prior estimates within a fraction of the process. For the experimental demonstration of the scheme presented here the inverse scheme is able to provide a low uncertainty real time prediction of filling time approximately 10 minutes after the initiation of the process, which corresponds to 30% of the whole duration.

The methodology developed here contributes toward the development of a probabilistic hybrid twin for composites manufacture. The integration of models and monitoring within an inverse solution allows the on-line estimation of the evolution of the process and its uncertainty. This can be utilized to carry out control and corrective actions during manufacturing potentially increasing process efficiency, improving part quality and reducing process failures and defects as well as reducing the resources required for inspection and quality assurance after the end of the process. The lineal character of the sensor, used in this study, lends itself to applications where continuous flow monitoring is appropriate, whereas simultaneous use of multiple sensors can provide the means for industrial control of flow processes in complex parts and geometries. The sensor flexibility can be used in monitoring of large scale carbon composite parts with complex geometries that is, double curvature without requiring tool modifications. A set of lineal flow sensors can be used to provide a 2-D filling map in real time with high accuracy. An optimization scheme can be applied identifying the optimal trade-off between the number of embedded sensors and the sensitivity of the monitoring system.

ACKNOWLEDGEMENTS

This work was supported by the EU through the Clean Sky 2 project SimCoDeQ (project ID: 686493). Data underlying this study can be accessed through the Cranfield University repository at https://doi.org/10.17862/cranfield.rd.7167896.

ORCID

K. I. Tifkitsis https://orcid.org/0000-0001-7367-1647
A. A. Skordos https://orcid.org/0000-0003-1273-029X

REFERENCES

[1] T. S. Mesogitis, A. A. Skordos, A. C. Long, *Compos. Part A Appl. Sci. Manuf.* **2014**, *57*, 67. https://doi.org/10.1016/j.compositesa.2013.11.004.

[2] E. B. Belov, S. V. Lomov, I. Verpoest, T. Peters, D. Roose, R. S. Parnas, *Compos. Sci. Technol.* **2004**, *64*, 1069. https://doi.org/10.1016/j.compscitech.2003.09.015.

[3] K. Hoes, D. Dinescu, H. Sol, R. S. Parnas, S. Lomov, *Compos. Part A Appl. Sci. Manuf.* **2004**, *35*, 1407. https://doi.org/10.1016/j.compositesa.2004.05.004.

[4] K. Hoes, D. Dinescu, H. Sol, M. Vanheule, R. S. Parnas, Y. Luo, I. Verpoest, *Compos. Part A Appl. Sci. Manuf.* **2002**, *33*, 959. https://doi.org/10.1016/S1359-835X(02)00035-0.

[5] A. Endruweit, P. McGregor, A. C. Long, M. S. Johnson, *Compos. Sci. Technol.* **2006**, *66*, 1778. https://doi.org/10.1016/j.compscitech.2005.10.031.

[6] A. Endruweit, F. Gommer, A. C. Long, *Compos. Part A Appl. Sci. Manuf.* **2013**, *49*, 109. https://doi.org/10.1016/j.compositesa.2013.02.012.

[7] F. Zhang, S. Comas-Cardona, C. Binetruy, *Compos. Sci. Technol.* **2012**, *72*, 1368. https://doi.org/10.1016/j.compscitech.2012.05.008.

[8] M. Matveev, F. Ball, I. Jones, A. Long, P. Schubel, M. Tretyakov, *J. Compos. Mater.* **2017**, *52*, 225. https://doi.org/10.1177/0021998317741951.

[9] R. Pan, Z. Liang, C. Zhang, B. E. N. Wang, *Polym. Compos.* **2000**, *21*, 996. https://doi.org/10.1002/pc.10253.

[10] K. I. Tifkitsis, A. A. Skordos, Integration of stochastic process simulation and real time process monitoring of LCM *SAMPE Conference 18, 11-13 September 2018, Southampton, UK* **2018**.

[11] F. Zhang, B. Cosson, S. Comas-Cardona, C. Binetruy, *Compos. Sci. Technol.* **2011**, *71*, 1478. https://doi.org/10.1016/j.compscitech.2011.06.006.

[12] B. Markicevic, D. Heider, S. G. Advani, S. Walsh, *Compos. Part A Appl. Sci. Manuf.* **2005**, *36*, 851. https://doi.org/10.1016/j.compositesa.2004.09.002.

[13] J. Li, C. Zhang, R. Liang, B. Wang, *Compos. Part A Appl. Sci. Manuf.* **2005**, *36*, 564. https://doi.org/10.1016/j.compositesa.2004.10.001.

[14] J. Li, C. Zhang, Z. Liang, B. Wang, *J. Manuf. Syst.* **2006**, *25*, 108. https://doi.org/10.1016/S0278-6125(06)80037-3.

[15] J. Guilleminot, M. Deléglise, C. Binetruy, P. Krawczak, Stochastic modeling of resin flow in fibrous media in liquid composite molding *16th International Conference on Composite Materials, 7-13 July 2007, Kyoto, Japan* **2007**.

[16] S. R. M. Kueh, S. G. Advani, R. S. Parnas, *Polym. Compos.* **2000**, *21*, 436. https://doi.org/10.1002/Pc.10200.

[17] A. A. Skordos, P. I. Karkanas, I. K. Partridge, *Meas. Sci. Technol.* **2000**, *11*, 25. https://doi.org/10.1088/0957-0233/11/1/304.

[18] C. Di Fratta, F. Klunker, F. Trochu, P. Ermanni, *Compos. Part A Appl. Sci. Manuf.* **2015**, *77*, 238. https://doi.org/10.1016/j.compositesa.2015.05.021.

[19] S. Konstantopoulos, H. Grössing, H. Patrick, M. Weninger, R. Schledjewski, *Polym. Compos.* **2018**, *39*, 360. https://doi.org/10.1002/pc.23944.

[20] W. Bai-Jian, C. Yu-Sung, Y. Yuan, F. Jun, *Polym. Compos.* **2016**, *37*, 1249. https://doi.org/10.1002/pc.23290.

[21] R. Matsuzaki, M. Shiota, *Compos. Part A Appl. Sci. Manuf.* **2016**, *84*, 43. https://doi.org/10.1016/j.compositesa.2016.01.006.

[22] C. Di Fratta, F. Klunker, P. Ermanni, *Compos. Part A Appl. Sci. Manuf.* **2013**, *47*, 1. https://doi.org/10.1016/j.compositesa.2012.11.008.

[23] A. A. Skordos, I. K. Partridge, *Inverse Probl. Sci. Eng.* **2004**, *12*, 157. https://doi.org/10.1080/10682760310001598616.

[24] Hexcel® HexForce G0926, Product Data www.hexcel.com**2018**.

[25] K. I. Tifkitsis, A. A. Skordos, *Compos. Part A Appl. Sci. Manuf.* **2019**, *123*, 180. https://doi.org/10.1016/j.compositesa.2019.05.014.

[26] S. Bickerton, S. G. Advani, *Compos. Sci. Technol.* **1999**, *59*, 2215. https://doi.org/10.1016/S0266-3538(99)00077-9.

[27] R. Meier, J. Heim, A. Nieratschker, S. Zaremba, K. Drechsler, Investigation of influencing parameters with respect to filling time in vibration assisted RTM processes *19th International Conference on Composite Materials, 28 July - 2 August 2013, Montreal, Canada* **2013**, 1.

[28] A. A. Skordos, Y. D. Kergomard, P. Marquette, P. de Luca, Methodology applied to integrate a viscosity model for liquid composites molding simulation in PAM-RTM® *ASME 2012 11th Biennial Conference on Engineering Systems Design and Analysis, July 2–4 2012, Nantes, France* **2012**, 1.

[29] M. A. Oliver, R. Webster, *Catena* **2014**, *113*, 56. https://doi.org/10.1016/j.catena.2013.09.006.

[30] M. D. McKay, B. WJC, *Technometrics* **1979**, *21*, 239. https://doi.org/10.2307/1268522.

[31] J. M. Lawrence, J. Barr, R. Karmakar, S. G. Advani, *Compos. Part A Appl. Sci. Manuf.* **2004**, *35*, 1393. https://doi.org/10.1016/j.compositesa.2004.05.002.

[32] K. I. Tifkitsis, T. S. Mesogitis, G. Struzziero, A. A. Skordos, *Compos. Part A* **2018**, *112*, 383. https://doi.org/10.1016/j.compositesa.2018.06.015.

[33] S. N. Lophaven, H. B. Nielsen, J. Søndergaard, *DACE-A Matlab Kriging toolbox, Version 2.0*, Informatics and Mathematical Modelling, Technical University of Denmark, DTU, Denmark **2002**, 1. https://orbit.dtu.dk/en/publications/dace-a-matlab-kriging-toolbox-version-20.

[34] T. D. Fadale, A. V. Nenarokomov, A. F. Emery, *Int. J. Heat Mass Transfer* **1995**, *38*, 511. https://doi.org/10.1016/0017-9310(94)00175-U.

[35] S. Somasundharam, K. S. Reddy, *Inverse Probl. Sci. Eng.* **2017**, *25*, 73. https://doi.org/10.1080/17415977.2016.1138946.

[36] R. Aster, B. Borchers, C. Thurber, *Parameter estimation and inverse problems*, 2nd, Academic Press, Cambridge, USA **2012**.

[37] G. O. Roberts, A. Gelman, W. R. Gilks, *Ann. Appl. Probab.* **1997**, *7*, 110. https://doi.org/10.1214/aoap/1034625254.

How to cite this article: Tifkitsis KI, Skordos AA. Real time uncertainty estimation in filling stage of resin transfer molding process. *Polymer Composites*. 2020;41:5387–5402. https://doi.org/10.1002/pc.25803

2020-09-24

Real time uncertainty estimation in filling stage of resin transfer molding process

Tifkitsis, Konstantinos

Wiley

Tifkitsis K, Skordos A. (2020) Real time uncertainty estimation in filling stage of resin transfer molding process. Polymer Composites, Volume 41, Issue 12, December 2020, pp. 5387-5402 https://doi.org/10.1002/pc.25803